A wave of minor *de novo* DNA methylation initiates in mouse 8-cell embryos and co-regulates imprinted X- chromosome inactivation

Yuan Yue[1], Wei Fu[1], Qianying Yang[1], Chao Zhang[1], Wenjuan Wang[1], Meiqiang Chu[1], Qingji Lyu[1], Yawen Tang[1], Jian Cui[1], Xiaodong Wang[1], Zhenni Zhang[1], Jianhui Tian[1], Lei An[1*]

[1] State Key Laboratory of Animal Biotech Breeding, National Engineering Laboratory for Animal Breeding; Key Laboratory of Animal Genetics, Breeding and Reproduction of the Ministry of Agriculture and Rural Affairs, College of Animal Science and Technology, China Agricultural University, Beijng, China.

*Authors for correspondence (anleim@cau.edu.cn)

Keywords: preimplantation embryos, *de novo* DNA methylation, DNA methyltransferase 3B, imprinted X chromosome inactivation, polycomb repressive complexes 2

Summary statement

A minor wave of *de novo* DNA methylation has been initiated prior to blastocyst formation, but not during the implantation period, and co-regulates imprinted X-chromosome inactivation.

ABSTRACT

DNA methylation is extensively reprogrammed during early stage of mammalian development and is essential for normal embryogenesis. It is well established that mouse embryos acquire genome-wide DNA methylation during implantation, referred to as *de novo* DNA methylation, from globally hypomethylated blastocysts. However, the fact that the main *de novo* DNA methyltransferase 3B (DNMT3B) is initially expressed as early as the 8-cell stage during preimplantation development, contradicts the current knowledge about timing of initiation of *de novo* DNA methylation. Here, we reported that a previously overlooked minor wave of *de novo* DNA methylation initially occurs during the transition from the 8-cell to blastocyst stage, before the well-known large-scale *de novo* DNA methylation during implantation. Bioinformatic and functional analyses indicated that minor *de novo* DNA methylation preferentially occurs on the X chromosome and co-regulates imprinted X-chromosome inactivation via the interaction between DNMT3B and polycomb repressive complexes 2 core components during blastocyst formation. Furthermore, minor *de novo* DNA methylation also finetunes proliferation, lineage differentiation and metabolic homeostasis of preimplantation embryos, and is critical for embryonic developmental potential and pregnancy outcomes. Thus, our study updates the current knowledge of embryonic *de novo* DNA methylation, thereby providing a novel insight of early embryonic epigenetic reprogramming.

INTRODUCTION

Mammalian early embryos are co-regulated by a series of spatiotemporally restricted epigenomic events that are critical for acquiring developmental potential. In mouse, it has been widely accepted that a wave of genome-wide *de novo* DNA methylation occurs around the time of implantation, thus re-establishing DNA methylation patterns from a globally hypomethylated blastocysts to relatively static DNA methylation patterns in post-implantation embryos (Borgel et al., 2010; Smith et al., 2012). DNA methyltransferase 3B (DNMT3B) is the main enzyme that catalyzes embryonic *de novo* DNA methylation. Genetic depletion of *Dnmt3b* results in hypomethylation and dysregulation of pluripotency genes, gastrulation genes, germline-specific genes, *etc* (Auclair et al., 2014; Borgel et al., 2010), thus causing

severe developmental defects and lethality after implantation (Li et al., 1992; Okano et al., 1999). However, despite its developmental importance, the exact timing of initiation of *de novo* DNA methylation remains largely elusive.

Although earlier results using high-throughput sequencing methods suggested that *de novo* DNA methylation occurs during the transition from blastocysts to early post-implantation embryos (Auclair et al., 2014; Borgel et al., 2010; Guo et al., 2014; Smith et al., 2012), our detection assays (Figure 1A,B) and other previous studies (Guenatri et al., 2013; Li et al., 2016) indicated that *Dnmt3b,* the main *de novo* DNA methyltransferase, is initially expressed as early as the 8-cell stage during preimplantation development. This fact creates a contradiction that challenges current knowledge about timing of initiation of embryonic *de novo* DNA methylation, and therefore raising the possibility that embryonic *de novo* DNA methylation may precede, but not follows, the blastocyst stage.

To test this possibility, we reanalyzed well-established genome-scale bisulfite sequencing data that profiles DNA methylation maps from the mouse preimplantation to post-implantation embryos (Smith et al., 2012), and found approximately one-third of genes gained promoter DNA methylation during the transition from the 8-cell to blastocyst stage. It means that despite global DNA demethylation throughout the preimplantation development, a small proportion of regions have initiated *de novo* DNA methylation prior to the blastocyst stage, which we designated as minor *de novo* DNA methylation. We next ask its developmental functions for embryogenesis. Of interest, minor *de novo* DNA methylation is more prone to occur on the X chromosome. We next confirmed that minor *de novo* DNA methylation plays an important role in establishing imprinted X chromosome inactivation (iXCI) via the interaction between DNMT3B and the polycomb repressive complexes 2 (PRC2) core components, which are critical for X-linked heterochromatin. Further analyses indicated that minor *de novo* methylation also finetunes proliferation, lineage differentiation and metabolism of preimplantation embryos, and thus affecting the developmental potential and final pregnancy outcomes. Thus, our study provides a novel understanding of *de novo* DNA methylation during early development, which updates the current knowledge of embryonic epigenomic hallmark events and their interactions.

RESULTS AND DISCUSSION

A small proportion of promoters initiate *de novo* DNA methylation by the 8-cell stage

To investigate the earliest initiation of *de novo* DNA methylation, we first examined the expression patterns of *Dnmt3s* in mouse preimplantation embryos. Results from previously published transcriptome (Fan et al., 2015) and our quantitative RT-PCR (qRT-PCR) detection showed that expression of *Dnmt3b*, the main enzyme for embryonic *de novo* DNA methylation (Borgel et al., 2010; Okano et al., 1999), as well as its non-catalytic partner *Dnmt3l* (Gowher et al., 2005), initiated by the 8-cell stage, and were further increased upon preimplantation development (Figure 1A). By contrast, the expression of *Dnmt3a*, which is mainly required for gametic methylation (Kaneda et al., 2004a), was maintained at low levels concurrently (Figure 1A). The initial expression of *Dnmt3b* was also confirmed at the protein level. Nuclear location of DNMT3B can be clearly detected from the 8-cell stage onward (Figure 1B). Given the essential role of DNMT3B in catalyzing *de novo* DNA methylation, we postulated that embryonic *de novo* DNA methylation may initiate as early as the 8-cell stage, which challenges current knowledge that *de novo* DNA methylation initiates during implantation.

To test the hypothesis, we next reanalyzed a well-established genome-scale bisulfite sequencing data that profiles DNA methylation maps from the mouse preimplantation to post-implantation stage (Smith et al., 2012). We first focused our analysis on DNA methylation dynamics of promoter, the preferential target of DNMT3B (Auclair et al., 2014; Borgel et al., 2010), from the 8-cell stage onward. Despite the global loss of promoter DNA methylation (Figure 1—figure supplement 1A), more detailed characterization showed that a considerable proportion of promoters (approximately 30%) gained DNA methylation during the transition from the 8-cell to blastocyst stage, even though most promoters underwent demethylation (Figure 1C). In line with this, a small proportion of gene bodies also gained DNA methylation during the transition (Figure 1D). This observation was also supported by reanalysis results (Figure 1—figure supplement 1B) of another published bisulfite sequencing data (Smith et al., 2017). By tracking DNA methylation dynamics of two subsets of promoters

that gained or lost DNA methylation from the 8-cell to blastocyst stage respectively, we found promoters that underwent demethylation were relatively hypermethylated following fertilization, and then were gradually demethylated until reaching their lowest value in ICM (Figure 1E). In contrast, promoters that gained DNA methylation by the 8-cell to blastocyst stage, were more hypomethylated following fertilization, and reached their lowest DNA methylation levels at the 8-cell stage (Figure 1F). Given the hypomethylated regions are more accessible to *de novo* methyltransferases (Lorincz et al., 2002), this subset of promoters may be targeted by DNMT3B at the 8-cell stage and thus initiate their *de novo* DNA methylation before the blastocyst stage, and then continued during implantation (Figure 1F). As exemplified by the *Yy2* promoter, the results of PCR-based bisulfite sequencing further confirmed the occurrence of *de novo* methylation before the blastocyst stage (Figure 1G). To distinguish two waves of *de novo* DNA methylation before and after the blastocyst stage, we designated them as minor and major *de novo* DNA methylation, respectively. We noticed that, besides of many important basic processes common to two waves of *de novo* DNA methylation, minor *de novo* DNA methylation may be linked to chromosome organization (Figure 1H). Compared with conventionally accepted major *de novo* DNA methylation, minor *de novo* DNA methylation showed a smaller increase in promoter DNA methylation that tended to occur in low CpG-containing promoters (Figure 1—figure supplement 1C,D).

Minor *de novo* DNA methylation preferentially occurs on the X chromosome and plays an important role in iXCI

To obtain a global view of minor *de novo* DNA methylation, we next detected the chromosome-wide distribution of *de novo* methylated promoters from the 8-cell to ICM, and found that they were globally distributed across autosomes, with the percentage ranging from 23% to 33% (Figure 2A-B). Of note, approximately half of X-linked promoters (48%) underwent minor *de novo* DNA methylation throughout the X chromosome (Figure 2—figure supplement 1A), much higher than those of autosomal promoters (Figure 2B). This result was similar with that of major *de novo* DNA methylation during implantation (Figure 2—figure supplement 1B,C). The X chromosome-biased prevalence of *de novo* DNA methylation is reminiscent of XCI, a female-specific epigenetic event that occurs during early development for balancing the X-linked gene dosage between males and females. In mice, early embryos

undergo two waves of XCI: iXCI initiates in early preimplantation embryos and persists in extraembryonic tissues, and rXCI occurs in the embryonic cells by implantation stage (Augui et al., 2011; Chow and Heard, 2009; Lee and Bartolomei, 2013). Spatiotemporal co-occurrence of minor *de novo* DNA methylation and iXCI on the X chromosome, led us to ask if these two epigenetic events are functional linked during preimplantation development. Indeed, it has been well-accepted DNA methylation is essential for maintaining X chromosome-wide transcriptional silence of rXCI during implantation (Blewitt et al., 2008; Sado et al., 2000), its role in iXCI has been documented as a long-standing open question of epigenetic programming during preimplantation development (Csankovszki et al., 2001; Kaneda et al., 2004b; Sado et al., 2000; Sado et al., 2004). Given identification of biological function of minor *de novo* DNA methylation requires that only minor, but not major *de novo* methylation, is functionally inactivated before blastocyst formation, we next transiently inhibited *Dnmt3b* via siRNA-mediated knockdown (KD). As expected, *Dnmt3b* mRNA and protein levels were significantly reduced in morulae, but not in blastocysts compared to those of the negative control (NC) group (Figure 2—figure supplement 2A-C). The transient inhibition of *Dnmt3b* resulted in a significant decrease in the global level of 5mC staining before blastocyst formation (Figure 2—figure supplement 2D,E). We next detected the H3K27me3, a classic marker for establishment of XCI achieving X chromosome-wide heterochromatinization of transcriptional depression (Chow and Heard, 2009; Huynh and Lee, 2005; Wutz, 2011). In line with the decreased DNA methylation levels (Figure 2—figure supplement 2D,E), we found all detected *Dnmt3b*-KD female blastocysts contained trophoblast cells lacking the H3K27me3 domain, with a variable frequency ranging from 10.7% to 42.4%; whereas nearly all NC female blastocysts showed a single H3K27me3 domain in each trophoblast (Figure 2C,D), indicating *Dnmt3b* deficiency leads to an impaired iXCI in preimplantation female embryos. Next, we further confirmed this result via *Dnmt3b*-knockout (KO) and chemical-induced inhibition of DNMT3B (Figure 2—figure supplement 2F,G). In addition, the involvement of minor *de novo* DNA methylation in iXCI establishment was further supported by the fact that many representative X-linked non-escaping genes tended to *de novo* methylated during the transition from the 8-cell to ICM (Figure 2—figure supplement 2H). Although previous studies have described that loss of maintenance methyltransferase

Dnmt1, or *de novo* DNA methyltransferases *Dnmt3a* and *Dnmt3b* in the female germ line, had no effect on iXCI in the trophoblast (Kaneda et al., 2004b; Sado et al., 2000), authors also emphasized that the role of *de novo* methylation in iXCI, remains an open question, possibly due to heterozygous deletion of *Dnmt3a/3b* in the maternal germ line, but not in preimplantation embryos (Kaneda et al., 2004b). This is partially in line with another previous report showing a significantly higher expression of *Pgk1*, a representative X-linked non-escaping gene, in *Dnmt3a*/*3b*-deficient female embryos (Sado et al., 2004). Taken together, our data from multiple methodologies, provided direct evidence that a wave of minor *de novo* DNA methylation preceding the blastocyst stage, is critical for establishing iXCI.

Minor *de novo* DNA methylation co-regulates iXCI via the interaction between DNMT3B and PRC2 core components

Having confirmed the functional role of minor *de novo* methylation in iXCI, we next attempt to explore the underlying mechanism. Because iXCI is initiated by *Xist* RNA upregulation and coating during the 8-cell and morular stage (Penny et al., 1996), we first detected *Xist* mRNA expression. No significant difference in the degrees of absence of the *Xist* domain in each blastomere nucleus between NC and *Dnmt3b*-KD female morulae (Figure 3A,B), which were also confirmed by detecting *Dnmt3b*-KO female morulae (Figure 3—figure supplement 1). In line with this, single female embryo qRT-PCR analysis of *Xist* and its essential upstream activator *Rnf12* during initial stage of iXCI, showed that the expression levels of *Xist* and *Rnf12* were not affected by *Dnmt3b* deficiency (Figure 3C). Our results demonstrate that minor *de novo* DNA methylation participates in establishment, but not in initiation of iXCI.

In attempt to further understand the mechanism underlying the role of minor *de novo* DNA methylation in establishing iXCI, we next asked whether the *Dnmt3b* deficiency-induced loss of H3K27me3 domains was related to abnormal expression of histone-modifying enzymes. We detected the expression of H3K27 histone methyltransferases or the partner (*Ezh2*, *Suz12, Eed*) and demethylase (*Kdm6a*, *Kdm6b*). The results showed *Dnmt3b* deficiency has no impact on the expression of these enzymes (Figure 3D). Given DNA methylation has a synergistic relationship with H3K27me3 in the process of heterochromatin formation

200 (Hagarman et al., 2013; King et al., 2016), we reanalyzed H3K27me3 dynamics of promoters
201 that underwent minor *de novo* DNA methylation during the transition from the 8-cell to ICM
202 using a well-established H3K27me3 ChIP-seq data (Liu et al., 2016). As expected, concurrent
203 increase in H3K27me3 enrichment can be clearly observed throughout the X chromosome
204 and many *de novo* methylated X-linked promoters (Figure 3—figure supplement 2A,B). Next,
205 we used *in situ* proximity ligation assays (PLA), a method that is suitable for visualizing
206 protein interactions (Soderberg et al., 2006) to detect direct interactions between DNMT3B
207 and PRC2 core components, *i.e.,* EZH2, SUZ12, EED, which are essential for X-linked
208 heterochromatin. It is clearly visible that DNMT3B-EZH2, DNMT3B-SUZ12 and
209 DNMT3B-EED interactions can be detected in the nuclei by the blastocyst stage (Figure 3E).
210 In line with this, the function of *de novo* DNA methylation in XCI, as well as direct
211 interaction between DNMT3B and PRC2 core components (Figure 3F,G; Figure 3—figure
212 supplement 3A-G), were also confirmed in differentiated female ES cells. Collectively, our
213 results support the idea that minor *de novo* DNA methylation plays an important role in iXCI
214 via synergistic interaction with heterochromatic histone modifications, rather than
215 transcriptional regulation of iXCI-regulating genes.

216 **Minor *de novo* DNA methylation participates in embryonic proliferation,**
217 **differentiation and affects developmental potential**

218 It has been known that *de novo* DNA methylation during implantation stage plays an essential
219 role in transcriptional regulation of developmental genes that are critical for embryonic
220 differentiation and survival (Auclair et al., 2014; Borgel et al., 2010), thus we next attempted
221 to test the additional short-and long-term developmental consequences of minor *de novo* DNA
222 methylation. Thus, we performed an integrated analysis using the published bisulfite
223 sequencing data (Smith et al., 2012) and transcriptome data (Wu et al., 2016) that profiles
224 DNA methylation and gene expression maps from the 8-cell to ICM, respectively. Putative
225 genes transcriptionally regulated by minor *de novo* DNA methylation (Figure 4—figure
226 supplement 1A) were functionally related to many basic processes that were critical for
227 normal embryonic survival, development and postnatal growth (Figure 4—figure supplement
228 1B,C), while genes subject to DNA demethylation also participate in similar processes
229 (Figure 4—figure supplement 1D), suggesting the developmental significance of DNA

methylation homeostasis.

Given identification of long-term developmental consequence of minor *de novo* DNA methylation requires that only minor, but not major *de novo* methylation, is functionally inactivated before blastocyst formation, we next used transient *Dnmt3b*-KD (Figure 2—figure supplement 2A-E) to examine whether minor *de novo* methylation is functionally associated with these basic biological processes before blastocyst formation and in turn affects developmental potential and pregnancy outcomes. *Dnmt3b* deficiency not only inhibited proliferation (Figure 4A), but also changed lineage differentiation of blastocysts (Figure 4B). Next, we examined the energy metabolism of *Dnmt3b*-KD embryos. Despite the unchanged total ATP production, *Dnmt3b* deficiency led to a significantly disruption in oxidative phosphorylation (OXPHOS)-dependent-ATP production (Figure 4C). These observations were further confirmed via chemical-induced inactivation of *de novo* DNA methylation (Figure 4—figure supplement 2A-C). Finally, we transferred *Dnmt3b*-KD embryos into pseudopregnant recipient females. Compared with that in NC group, *Dnmt3b*-KD embryos resulted in a significantly reduced implantation rate and live birth rate (Figure 4D-E), suggesting the important role of minor *de novo* DNA methylation in influencing embryonic developmental potential. Since knockdown-mediated *Dnmt3b* deficiency has been restored to normal levels at the blastocyst stage, the possibility can be excluded that the reduced implantation rate and live birth rate may be due to defective major *de novo* DNA methylation. Similarly, previous studies using *Tet1*-deficient or *Tet1*/*3*-deficient embryos, indicated the critical role of TET-mediated DNA demethylation in these processes, as well as embryonic and postnatal development (Dawlaty et al., 2011; Ito et al., 2010; Kang et al., 2015). Thus, it can be presumed that minor *de novo* DNA methylation, and TET-mediated demethylation, may synergistically co-regulate DNA methylation homeostasis before blastocyst formation, thus fine-tuning embryonic developmental potential and long-term outcomes.

It is also worth mentioning that minor *de novo* DNA methylation is definitely distinct from previously reported DNA re-methylation in monkey and human preimplantation embryos, which occurs during the 2- to 8-cell and 4- to 8-cell transition respectively (Gao et al., 2017; Guo et al., 2014; Zhu et al., 2018). The so-called DNA re-methylation does not occur in naturally conceived mouse embryos. However, an aberrant wave of DNA re-methylation has

been identified in cloned mouse preimplantation embryos as an epigenetic barrier that impairs full-term developmental potential (Gao et al., 2018).

Collectively, our study presents an update on the current knowledge of embryonic *de novo* DNA methylation. We identified that a wave of minor *de novo* DNA methylation has initially occurred during the transition from the mouse 8-cell to blastocyst stage, but not during the implantation stage. Of interest, we provide the first evidence that DNA methylation is important for establishing iXCI in preimplantation female embryos. Our data, together with previous results, also support a model where minor *de novo* DNA methylation and demethylation co-orchestrate DNA methylation homeostasis before blastocyst formation, and serve as epigenetic mechanisms affecting embryonic developmental potential by fine-tuning the processes of lineage commitment, proliferation and metabolic homeostasis (Figure 4F). Thus, our work provides a novel insight for understanding epigenetic programming and reprogramming during early embryonic development.

MATERIALS AND METHODS

Mouse embryo preparation

All experimental procedures were approved by and performed in accordance with the guidelines of the Institutional Animal Care and Use Committee of China Agricultural University. Mice were fed ad libitum and housed under controlled lighting (12 light:12 dark) and specific pathogen-free conditions. ICR female mice were superovulated with 5 IU pregnant mare serum gonadotrophin (PMSG; Ningbo Hormone Product Co., Ltd, Ningbo, China) and a further 5 IU human chorionic gonadotropin (hCG; Ningbo Hormone Product CO., Ltd) 46-48 h later. Then, superovulated ICR females were cogaged individually with ICR males. *In vivo* zygote, 2-cell embryos, 4-cell embryos, 8-cell embryos, morulae, or blastocysts were flushed from oviducts and uterus at 16 h, 42 h, 54 h, 66 h, 78 h, or 93 h post-hCG, respectively.

Quantitative real-time PCR analysis

Total RNA was extracted from embryos using TRIzol^{TM} (Invitrogen, Carlsbad, CA, USA). RNA was treated with DNase, and reverse-transcribed into cDNA using the HiScript II Q Select RT Kit (Vazyme, Nanjing, China). qRT-PCR was performed using SsoFast Eva Green

290 Supermix (Bio-Rad, Hercules, CA, USA). The relative expression data were calculated using
291 the $2^{-\Delta Ct}$ method. Relative expression level was normalized to the housekeeping gene *H2afz*,
292 and each experiment was repeated at least three times, as previously reported. Primers used
293 are listed in Table S1.

294 For qRT-PCR on single female or male embryo, a blastomere was isolated and treated with
295 2 μL Cells-to-cDNA™ II Cell Lysis Buffer (Invitrogen) at 75°C for 15 min. Next, the lysate
296 was digested with proteinase K (Merck, Kenilworth, NJ, USA) at 55°C for 2 h, and used for
297 sex determination according to the manufacturer's instruction of Ex Taq Hot Start Version
298 (Takara Bio, Shiga, Japan). The amplification was conducted as follows: 95 °C for 3 min; 40
299 cycles of 95 °C for 10 s, 52 °C for 15 s, 72 °C for 15 s; and extension at 72 °C for 5 min. The
300 remaining part of embryo was treated with 5 μL Cells-to-cDNA™ II Cell Lysis Buffer
301 (Invitrogen), and then reverse-transcribed into cDNA with the HiScript II Q Select RT Kit
302 (Vazyme).

303 **Immunofluorescence analysis**

304 Embryos were fixed with 4% Paraformaldehyde (PFA) in PBS-0.1% PVA at 4 °C overnight.
305 After permeabilizing with 0.5% Triton X-100 in PBS-0.1%PVA (PBST-PVA) for 1 h at room
306 temperature, embryos were blocked with 1% BSA in PBST-PVA at 4 °C for 6 h. Embryos
307 were incubated with primary anti-DNMT3B antibody (1:200; GeneTex, Irvine, CA, USA),
308 anti-H3K27me3 antibody (1:1000; MilliporeSigma, Burlington, MA, USA), or anti CDX2
309 antibody (1:200; BioGenex, Fremont, CA, USA) overnight at 4 °C, followed by Alexa
310 Fluor-488 (anti-mouse; Invitrogen) and Alexa Fluor-594 (anti-rabbit; Invitrogen) labeled
311 secondary antibodies for 1 h at room temperature. Finally, embryos were counterstained with
312 DAPI. Fluorescence images were obtained under an upright microscope (BX51; Olympus)
313 using an attached digital microscope camera (DP72; Olympus). Quantification of the
314 immunofluorescence results were performed using Image J (National Institutes of Health,
315 Bethesda, MD, USA).

316 For 5-methylcytosine (5-mC) staining, permeabilized embryos were treated with 4 M HCl
317 for 10 min and 100 mM Tris-HCl for 10 min at room temperature, and then blocked overnight
318 at 4 °C. Next, embryos were incubated with primary anti-5mC antibody (1:200; Active Motif,
319 Carlsbad, CA, USA) at room temperature for 2 h, followed by secondary antibody for 1 h.

320 Furthermore, embryos for sex determination were removed from the slides and digested
321 with Cells-to-cDNA™ II Cell Lysis Buffer (Invitrogen) and proteinase K (Merck) as
322 described above, followed by sex determination and genotyping using PCR. The primer
323 sequences are listed in Table S1.

324 **Bisulfite sequencing**

325 The DNA methylation profile was analyzed by PCR-based bisulfite sequencing. 40 IVO
326 blastocysts or 80 8-cell embryos were digested and bisulfite converted according to the
327 manufacturer's instruction of EZ DNA Methylation-Direct Kit (Zymo, Irvine, CA, USA).
328 Bisulfite-specific primers were designed with the online Methyl Primer Express, v1.0
329 (http://www.urogene.org/methprimer/ Table S1). The converted DNA was amplified by PCR
330 using Ex Taq Hot Start Version (Takara). And the PCR products were subcloned into
331 pEASY-T5 Zero Cloning Kit (TransGen, Beijing, China). At least 10 clones per group were
332 sequenced. The sequencing results were analyzed with QUMA (http://quma.cdb.riken.jp/).

333 **Microinjection of siRNA**

334 siRNA oligo sequences were synthesized by GenePharma (Shanghai, China). The sequences
335 of *Dnmt3b* siRNA used in the present study were as follows: sense
336 5'-CCUCAAGACAAAUAGCUAUTT-3', antisense
337 5'-AUAGCUAUUUGUCUUGAGGTT-3'. siRNA was diluted to 100 μM and stored at
338 -80 °C. For siRNA microinjection, 5 pL siRNA was microinjected into the cytoplasm of
339 zygotes. Then embryos were cultured in KSOM at 37 °C under 5% CO_2 and collected at the
340 8-cell, morula or blastocyst stage for further analyses.

341 **RNA-FISH**

342 RNA-FISH was performed using ViewRNA™ ISH Cell Assay Kit (Invitrogen) according to
343 the manufacturer's instructions. Fixed embryos were treated with Detergent Solution QC at
344 room temperature for 5 min, and digested with protease QS at room temperature for 10 min.
345 Next, the embryos were hybridized with probes against *Xist* (Invitrogen) at 40 °C for 3 h.
346 Then the embryos were hybridized with PreAmplifier and Amplifier Mix at 40 °C for 30 min,
347 respectively. Label Probe Mix was used to produce a signal. The embryos were
348 counterstained with DAPI, and imaged using an attached digital microscope camera (DP72;
349 Olympus).

350 **Proximity ligation assays**

351 The in situ proximity ligation assays (PLA) was performed using the Duolink® In Situ Red
352 Starter Kit according to the manufacturer's instruction (MilliporeSigma). Embryos were fixed
353 and permeabilized as described for immunofluorescence. After blocking, embryos were
354 incubated with primary antibody. Embryos were then incubated with PLA probes, followed
355 by ligation and amplification reaction. Finally, embryos were counterstained with Duolink®
356 In Situ Mounting Medium with DAPI (MilliporeSigma). Furthermore, DNMT3B, EZH2,
357 SUZ12, or EED single primary antibody, and secondary antibodies alone were used as
358 technical negative controls.

359 **Generation of Dnmt3a/Dnmt3b KO ESC**

360 Mouse ESCs line PGK12.1 was used in the present study. Cells were cultured in KnockOut™
361 DMEM medium (Invitrogen) containing 10% fetal bovine serum (VISTECH, Sydney,
362 Australia), 2mM GlutaMAX (Invitrogen), 1×non-essential amino acid (MilliporeSigma), 55
363 μM β-mercaptoethanol (Invitrogen), 1000 units/ml mouse recombinant leukemia inhibitor
364 factor (MilliporeSigma), 100 units/ml penicillin and 100 μg/ml streptomycin (both
365 Invitrogen). To induce ESC differentiation, ESCs were cultured in DMEM/F12 (Invitrogen)
366 and Neurobasal medium supplement with B27 and N2 supplement (Invitrogen), 100 units/ml
367 penicillin-streptomycin (Invitrogen).

368 Knockout of *Dnmt3b* or *Dnmt3a* for ES cells was performed using CRISPR/Cas9n. sgRNA
369 was designed using Benchling (https://www.benchling.com/). sgRNAs were constructed to
370 pSpCas9n(BB)-2A-Puro vector (PX462, Addgene plasmid no. 62987). 4 μg of the plasmid
371 was transfected using Lipofectamine 2000 (Invitrogen) according to the manufacturer's
372 protocol. 2 μg/ml puromycin (Solarbio, Beijing, China) was used to selected the positive
373 colonies. After selection, colonies were picked out and expanded. Cells were verified by
374 genotyping and Sanger sequencing. The sgRNA sequences and knockdown cell detection
375 primers are listed in Table S1.

376 **Co-immunoprecipitation**

377 Co-immunoprecipitation (Co-IP) was performed with Dynabeads™ Protein G
378 Immunoprecipitation Kit (Invitrogen) according to the manufacturer's protocol. Briefly, 3 μg
379 DNMT3B antibody (GeneTex) or mouse IgG (MilliporeSigma) was incubated to Protein G

380 beads with rotation for 10 minutes at room temperature. The beads were washed with
381 Washing Buffer. Then cell lysates were then incubated with the beads-antibody complex with
382 rotation for 4h at 4 °C. Then the beads were washed 3 times with Washing Buffer, and were
383 eluted with loading buffer by heating at 98 °C for 10min. Co-IP products were analyzed by
384 western blot using the indicated primary antibodies and secondary antibodies. And protein
385 bands were detected with Tanon 5200 detection systems (Tanon, Shanghai, China).

386 **Bioinformatics analysis**

387 Gene ontology (GO) annotation analysis was performed using Database for Annotation,
388 Visualization and Integrated Discovery (DAVID 6.8: https://david.ncifcrf.gov/). Heatmaps
389 were plotted using the R software "pheatmap" package (version 1.0.12). The integrative
390 genomics viewer (IGV) was used to visualize the ChIP-seq results. The phenotype of genes
391 was analyzed on the Mouse Genome Informatics (MGI; http://www.informatics.jax.org/)
392 database.

393 **EdU assay**

394 The proliferation of embryos was detected with a BeyoClick™ EdU-594 Cell Proliferation
395 Kit (Beyotime, Shanghai, China) according to the manufacturer's instruction. Embryos were
396 incubated in EmbryoMax® KSOM Mouse Embryo Media (MilliporeSigma) containing 10
397 μM EdU at 37 °C for 2 h, and then fixed and permeabilized. Afterwards, embryos were
398 incubated with the Click Reaction mixture for 2 min at room temperature before stained with
399 DAPI. Images were acquired under an upright microscope (BX51; Olympus) using an
400 attached digital microscope camera (DP72; Olympus).

401 **ATP measurement**

402 ATP level was measured using an ATP determination kit according to the manufacturer's
403 instruction (Beyotime). Briefly, blastocysts were incubated with M2 medium, and 1 μM
404 oligomycin (Abmore, Houston, USA) or 1 mM sodium oxamate (MilliporeSigma) in M2
405 medium at 37 °C for 15 min, respectively. Next, embryos were digested with 20 μL ATP lysis
406 buffer on ice, and the lysate was added to 96-well plates containing 100 μL ATP detection
407 working dilution. The luminescence was detected by a multifunctional microplate reader
408 (Infinite F200; TECAN, Mannedorf, Switzerland).

409 **Embryo transfer**

Pseudo-pregnant ICR females were mated with ICR males 3.5 d before embryo transfer. Blastocysts derives from NC or *Dnmt3b*-KD group were transferred to the uterine horn of pseudo-pregnant female mice.

Statistical analysis

All data are presented as mean ± SD and analyzed with the student's *t* test or correct χ^2 procedure by using SPSS v.25.0 (IBM, Armonk, NY, USA). Values of $P < 0.05$ were considered statistically significant.

Data availability

All data are available in the article and/or supporting information.

Acknowledgements

We thank Neil Brockdorff (University of Oxford) and Ingolf Bach (University of Massachusetts Medical School) for the gift and delivery of PGK12.1 cells. This work was supported by grants from the National Agriculture Key Science & Technology Project (NK20221201), Ningbo Major Science and Technology Project (2021Z112), the National Key R&D Program (2022YFD1300301).

Author contributions

Y.Y., J.T. and L.A. conceived and designed the experiments. Y.Y. C.Z. and W.W. were responsible for animal care and management. Y.Y., W.F., Q.Y., C.Z., W.W., M.C., Q.L., Y.T., J.C., X.W. and Z.Z. performed the experiments. Y.Y., W.F., J.T. and L.A. analyzed the data. Y.Y., W.F., J.T. and L.A wrote, and finalized the manuscript. All authors approved the paper.

Competing interests

The authors declare no competing interests.

References

Auclair, G., Guibert, S., Bender, A. and Weber, M. (2014). Ontogeny of CpG island

methylation and specificity of DNMT3 methyltransferases during embryonic development in the mouse. *Genome Biol* **15**, 545.

Augui, S., Nora, E. P. and Heard, E. (2011). Regulation of X-chromosome inactivation by the X-inactivation centre. *Nat Rev Genet* **12**, 429-442.

Blewitt, M. E., Gendrel, A. V., Pang, Z., Sparrow, D. B., Whitelaw, N., Craig, J. M., Apedaile, A., Hilton, D. J., Dunwoodie, S. L., Brockdorff, N., et al. (2008). SmcHD1, containing a structural-maintenance-of-chromosomes hinge domain, has a critical role in X inactivation. *Nat Genet* **40**, 663-669.

Borgel, J., Guibert, S., Li, Y., Chiba, H., Schubeler, D., Sasaki, H., Forne, T. and Weber, M. (2010). Targets and dynamics of promoter DNA methylation during early mouse development. *Nat Genet* **42**, 1093-1100.

Chow, J. and Heard, E. (2009). X inactivation and the complexities of silencing a sex chromosome. *Curr Opin Cell Biol* **21**, 359-366.

Csankovszki, G., Nagy, A. and Jaenisch, R. (2001). Synergism of Xist RNA, DNA methylation, and histone hypoacetylation in maintaining X chromosome inactivation. *J Cell Biol* **153**, 773-784.

Dawlaty, M. M., Ganz, K., Powell, B. E., Hu, Y. C., Markoulaki, S., Cheng, A. W., Gao, Q., Kim, J., Choi, S. W., Page, D. C., et al. (2011). Tet1 is dispensable for maintaining pluripotency and its loss is compatible with embryonic and postnatal development. *Cell Stem Cell* **9**, 166-175.

Fan, X., Zhang, X., Wu, X., Guo, H., Hu, Y., Tang, F. and Huang, Y. (2015). Single-cell RNA-seq transcriptome analysis of linear and circular RNAs in mouse preimplantation embryos. *Genome Biol* **16**, 148.

Gao, F., Niu, Y., Sun, Y. E., Lu, H., Chen, Y., Li, S., Kang, Y., Luo, Y., Si, C., Yu, J., et al. (2017). De novo DNA methylation during monkey pre-implantation embryogenesis. *Cell Res* **27**, 526-539.

Gao, R., Wang, C., Gao, Y., Xiu, W., Chen, J., Kou, X., Zhao, Y., Liao, Y., Bai, D., Qiao, Z., et al. (2018). Inhibition of Aberrant DNA Re-methylation Improves Post-implantation Development of Somatic Cell Nuclear Transfer Embryos. *Cell Stem Cell* **23**, 426-435 e425.

Gowher, H., Liebert, K., Hermann, A., Xu, G. and Jeltsch, A. (2005). Mechanism of stimulation of catalytic activity of Dnmt3A and Dnmt3B DNA-(cytosine-C5)-methyltransferases by Dnmt3L. *J Biol Chem* **280**, 13341-13348.

Guenatri, M., Duffie, R., Iranzo, J., Fauque, P. and Bourc'his, D. (2013). Plasticity in Dnmt3L-dependent and -independent modes of de novo methylation in the developing mouse embryo. *Development* **140**, 562-572.

Guo, H., Zhu, P., Yan, L., Li, R., Hu, B., Lian, Y., Yan, J., Ren, X., Lin, S., Li, J., et al. (2014). The DNA methylation landscape of human early embryos. *Nature* **511**, 606-610.

Hagarman, J. A., Motley, M. P., Kristjansdottir, K. and Soloway, P. D. (2013). Coordinate regulation of DNA methylation and H3K27me3 in mouse embryonic stem cells. *PLoS One* **8**, e53880.

Huynh, K. D. and Lee, J. T. (2005). X-chromosome inactivation: a hypothesis linking ontogeny and phylogeny. *Nat Rev Genet* **6**, 410-418.

Ito, S., D'Alessio, A. C., Taranova, O. V., Hong, K., Sowers, L. C. and Zhang, Y. (2010). Role of Tet proteins in 5mC to 5hmC conversion, ES-cell self-renewal and inner cell mass specification. *Nature* **466**, 1129-1133.

Kaneda, M., Okano, M., Hata, K., Sado, T., Tsujimoto, N., Li, E. and Sasaki, H. (2004a). Essential role for de novo DNA methyltransferase Dnmt3a in paternal and maternal imprinting. *Nature* **429**, 900-903.

Kaneda, M., Sado, T., Hata, K., Okano, M., Tsujimoto, N., Li, E. and Sasaki, H. (2004b). Role of de novo DNA methyltransferases in initiation of genomic imprinting and X-chromosome inactivation. *Cold Spring Harb Symp Quant Biol* **69**, 125-129.

Kang, J., Lienhard, M., Pastor, W. A., Chawla, A., Novotny, M., Tsagaratou, A., Lasken, R. S., Thompson, E. C., Surani, M. A., Koralov, S. B., et al. (2015). Simultaneous deletion of the methylcytosine oxidases Tet1 and Tet3 increases transcriptome variability in early embryogenesis. *Proc Natl Acad Sci U S A* **112**, E4236-4245.

King, A. D., Huang, K., Rubbi, L., Liu, S., Wang, C. Y., Wang, Y., Pellegrini, M. and Fan, G. (2016). Reversible Regulation of Promoter and Enhancer Histone Landscape by DNA Methylation in Mouse Embryonic Stem Cells. *Cell Rep* **17**, 289-302.

Lee, J. T. and Bartolomei, M. S. (2013). X-inactivation, imprinting, and long noncoding RNAs in health and disease. *Cell* **152**, 1308-1323.

Li, E., Bestor, T. H. and Jaenisch, R. (1992). Targeted mutation of the DNA methyltransferase gene results in embryonic lethality. *Cell* **69**, 915-926.

Li, Y., Seah, M. K. and O'Neill, C. (2016). Mapping global changes in nuclear cytosine base modifications in the early mouse embryo. *Reproduction* **151**, 83-95.

Liu, X. Y., Wang, C. F., Liu, W. Q., Li, J. Y., Li, C., Kou, X. C., Chen, J. Y., Zhao, Y. H., Gao, H. B., Wang, H., et al. (2016). Distinct features of H3K4me3 and H3K27me3 chromatin domains in pre-implantation embryos. *Nature* **537**, 558-+.

Lorincz, M. C., Schubeler, D., Hutchinson, S. R., Dickerson, D. R. and Groudine, M. (2002). DNA methylation density influences the stability of an epigenetic imprint and Dnmt3a/b-independent de novo methylation. *Mol Cell Biol* **22**, 7572-7580.

Okano, M., Bell, D. W., Haber, D. A. and Li, E. (1999). DNA methyltransferases Dnmt3a and Dnmt3b are essential for de novo methylation and mammalian development. *Cell* **99**, 247-257.

Penny, G. D., Kay, G. F., Sheardown, S. A., Rastan, S. and Brockdorff, N. (1996). Requirement for Xist in X chromosome inactivation. *Nature* **379**, 131-137.

Sado, T., Fenner, M. H., Tan, S. S., Tam, P., Shioda, T. and Li, E. (2000). X inactivation in the mouse embryo deficient for Dnmt1: distinct effect of hypomethylation on imprinted and random X inactivation. *Dev Biol* **225**, 294-303.

Sado, T., Okano, M., Li, E. and Sasaki, H. (2004). De novo DNA methylation is dispensable for the initiation and propagation of X chromosome inactivation. *Development* **131**, 975-982.

Smith, Z. D., Chan, M. M., Mikkelsen, T. S., Gu, H., Gnirke, A., Regev, A. and Meissner, A. (2012). A unique regulatory phase of DNA methylation in the early mammalian embryo. *Nature* **484**, 339-344.

Smith, Z. D., Shi, J., Gu, H., Donaghey, J., Clement, K., Cacchiarelli, D., Gnirke, A., Michor, F. and Meissner, A. (2017). Epigenetic restriction of extraembryonic

lineages mirrors the somatic transition to cancer. *Nature* **549**, 543-547.

Soderberg, O., Gullberg, M., Jarvius, M., Ridderstrale, K., Leuchowius, K. J., Jarvius, J., Wester, K., Hydbring, P., Bahram, F., Larsson, L. G., et al. (2006). Direct observation of individual endogenous protein complexes in situ by proximity ligation. *Nat Methods* **3**, 995-1000.

Wu, J. Y., Huang, B., Chen, H., Yin, Q. Z., Liu, Y., Xiang, Y. L., Zhang, B. J., Liu, B. F., Wang, Q. J., Xia, W. K., et al. (2016). The landscape of accessible chromatin in mammalian preimplantation embryos. *Nature* **534**, 652-+.

Wutz, A. (2011). Gene silencing in X-chromosome inactivation: advances in understanding facultative heterochromatin formation. *Nat Rev Genet* **12**, 542-553.

Zhu, P., Guo, H., Ren, Y., Hou, Y., Dong, J., Li, R., Lian, Y., Fan, X., Hu, B., Gao, Y., et al. (2018). Single-cell DNA methylome sequencing of human preimplantation embryos. *Nat Genet* **50**, 12-19.

Figure legends

Figure 1. A small proportion of promoters initiate *de novo* DNA methylation by 8-cell stage. (A) The mRNA expression levels of *Dnmt3s* from the 2-cell to blastocyst stage. The left ordinate represents FPKM values of *Dnmt3s* from published transcriptome data (Fan et al., 2015), and the right ordinate represents relative expression levels detected by qRT–PCR. (B) Immunofluorescent staining of DNMT3B in mouse preimplantation embryos. Scale bars: 50 μm. (C-D) DNA methylation changes of promoters (C) and gene bodies (D) during the transition from the 8-cell to blastocyst stage. Left panel: heat map of DNA methylation levels at promoters or gene bodies. Right panel: general trends of promoters or gene bodies undergoing *de novo* methylation or demethylation, and their relative contribution to differentially methylated regions. (E-F) DNA methylation dynamics of promoters subject to demethylation (E) or *de novo* methylation (F) during the transition from the 8-cell to blastocyst stage (red and green lines, average methylation levels; colored space, 10th/ 90th percentile). (G) Bisulfite sequencing analysis of *Yy2* in the 8-cell embryos and blastocysts. Black and white circles represent methylated cytosines and unmethylated cytosines respectively. (H) A model illustrating two waves of *de novo* DNA methylation before and after the blastocyst stage, and their potential functions.

Figure 2. Minor *de novo* methylation preferentially occurs on the X chromosome and plays an important role in iXCI. (A) The chromosome-wide distribution of *de novo* methylated promoters with different fold changes (FC) during the transition from the 8-cell to blastocyst stage. (B) Percentage of *de novo* methylated promotors on each chromosome during the transition from the 8-cell to blastocyst stage. (C) Representative immunostaining for H3K27me3 (red) in the nuclei (DAPI) of NC and *Dnmt3b*-KD female blastocysts colabeled with CDX2 (green)-positive trophoblast cells. Scale bars: 50 μm. (D) The ratio of trophoblast cells classified by the number of H3K27me3 domains in each NC and *Dnmt3b*-KD female blastocysts. Each bar represents one female embryo. All data are presented as the mean ± SD of at least three independent experiments. $^{**}P < 0.01$. ns, not significant.

Figure 3. Minor *de novo* DNA methylation co-regulates iXCI via the interaction between DNMT3B and PRC2 core components. (A) Representative localization of *Xist* expression

detected by RNA-FISH in the nuclei (DAPI) of NC and *Dnmt3b*-KD female morulae. (B) The ratio of blastomere with *Xist* signal to the total number of blastomeres in each NC and *Dnmt3b*-KD female morulae. Each bar represents one female embryo. (C) *Rnf12* and *Xist* expression levels in individual *Dnmt3b*-KD female 8-cell embryos and morulae. (D) Expression of H3K27me3 methylases (*Ezh2, Suz12* and *Eed*) and demethylases (*Kdm6a* and *Kdm6b*) in individual *Dnmt3b*-KD female morulae. (E) Validation of the interaction between DNMT3B and PRC2 core components, *i.e.,* EZH2, SUZ12, EED, via *in situ* PLA. (F) Representative immunostaining for H3K27me3 (red) in the nuclei (DAPI) of wild-type, *Dnmt3b*-KO, and *Dnmt3a/3b* double knockout (DKO) female ES cells differentiated for 7 days, as well as the ratio of ES cells classified by the number of H3K27me3 domains. (G) Western blot showing immunoprecipitation of DNMT3B and EZH2, SUZ12, EED from differentiated female ES cells. All data are presented as the mean ± SD of at least three independent experiments. $^{**}P < 0.01$. ns, not significant. Scale bars: 50 μm (A, E); 20 μm (F).

Figure 4. Minor *de novo* DNA methylation participates in embryonic proliferation, differentiation and affects developmental potential. (A) EdU staining of NC and *Dnmt3b*-KD blastocysts. Right panel: the percentage of EdU-positive cells. (B) The total cell number (left panel) and the ratio of ICM/TE (right panel) in NC and *Dnmt3b*-KD blastocysts. (C) The total ATP production (left panel) and OXPHOS-dependent ATP production (right panel) in NC and *Dnmt3b*-KD blastocysts. (D-E) Implantation rate (D) and live birth rate (E) in NC and *Dnmt3b*-KD groups. All data are presented as the mean ± SD of at least three independent experiments. $^{*}P < 0.05$, $^{**}P < 0.01$. ns, not significant. Scale bars: 50 μm (A, B). (F) A model illustrating a wave of minor *de novo* DNA methylation that initiates during the transition from the mouse 8-cell to blastocyst stage. Minor *de novo* DNA methylation co-regulates iXCI via the interaction between DNMT3B and PRC2 core components, and fine-tunes the processes of lineage commitment, proliferation and metabolic homeostasis before blastocyst formation.

Figure 1—figure supplement 1. (A) Dynamics of global methylation during preimplantation embryos (blue line, average methylation levels; colored space, 10th/ 90th percentile). (B) General trends of CpG islands undergoing *de novo* methylation or demethylation, and their relative contribution to differentially methylated regions. (C) Number of *de novo* methylated promoters with different fold changes (FC) at each consecutive transition. (D) DNA methylation dynamics of promoters with different CpG-densities during consecutive transitions.

Figure 2—figure supplement 1. (A) The distribution of *de novo* methylated and demethylated promoters cross the X chromosome during the transition from the 8-cell to blastocyst stage. (B) The chromosome-wide distribution of *de novo* methylated promoters with different fold changes (FC) during the transition from the blastocyst to post-implantation stage. (C) Percentage of *de novo* methylated promoters on each chromosome during the transition from the blastocyst to post-implantation stage.

Figure 2—figure supplement 2. (A) Relative expression levels of *Dnmt3b* in NC and *Dnmt3b*-KD morulae and blastocysts. (B-C) Immunofluorescent staining (C) and quantification (D) of DNMT3B in NC and *Dnmt3b*-KD morulae and blastocysts. (D-E) Immunofluorescent staining (D) and quantification (E) of 5-mC in NC and *Dnmt3b*-KD morulae and blastocysts. (F) The ratio of trophoblast cells classified by the number of H3K27me3 domains in each wild-type and *Dnmt3b*-KO female blastocysts. Each bar represents one female embryo. (G) The ratio of trophoblast cells classified by the number of H3K27me3 domains in female blastocysts exposed or not exposed to 5-aza-2'-deoxycytidine (5-aza-dC) from the 8-cell to blastocyst stage. Each bar represents one female embryo. (H) The fold changes of promoter methylation levels of X-linked non-escaping genes from the 8-cell to blastocyst stage. All data are presented as the mean ± SD of at least three independent experiments. $*P < 0.05$, $**P < 0.01$. ns, not significant. Scale bars: 50 μm (B, D).

Figure 3—figure supplement 1. The ratio of blastomere with Xist signal to the total number of blastomeres in each wild-type and *Dnmt3b*-KO female morulae. Each bar represents one female embryo.

Figure 3—figure supplement 2. (A) H3K27me3 enrichment cross the X chromosome from

the 8-cell to blastocyst stage based on the previously published data (Liu et al., 2016). (B) Concurrent increase in H3K27me3 enrichment (left panel) and DNA methylation levels (right panel) at selected X-linked promoters that undergo minor *de novo* DNA methylation.

Figure 3—figure supplement 3. (A) Schematic illustration of generation of *Dnmt3b*-KO female ES cells via the CRISPR/Cas9n system. (B) Detection of deletion introduced by sgRNA-Cas9n targeting *Dnmt3b* via PCR with genomic DNA from wild-type and *Dnmt3b*-KO female ES cells. (C) Relative expression levels of *Dnmt3b* in wild-type and *Dnmt3b*-KO female ES cells. (D) Schematic illustration of generation of DKO female ES cells via the CRISPR/Cas9n system. (E) Detection of deletion introduced by sgRNA-Cas9n targeting *Dnmt3a/3b* via PCR with genomic DNA from wild-type and DKO female ES cells. (F) Relative expression levels of *Dnmt3a* and *Dnmt3b* in wild-type and DKO female ES cells. (G) Representative immunostaining for H3K27me3 (red) in the nuclei (DAPI) of wild-type, *Dnmt3b*-KO, and DKO female ES cells differentiated for 5 or 9 days, as well as the ratio of ES cells classified by the number of H3K27me3 domains. All data are presented as the mean ± SD of at least three independent experiments. $^{**}P < 0.01$. Scale bars: 20 μm.

Figure 4—figure supplement 1. (A) A scatter plots of changes in promoter DNA methylation and gene expression from the 8-cell embryos to ICM. Red plots indicate putative genes that undergo minor *de novo* DNA methylation (FC > 2) and are downregulated (FC < 0.5). (B-C) Gene ontology analysis (B) and phenotype annotation (C) of genes transcriptionally regulated by minor *de novo* DNA methylation. Blue squares indicate genes that are related to developmental or lethal phenotypes. (D) Gene ontology analysis of genes transcriptionally regulated by DNA demethylation from the 8-cell embryos to ICM.

Figure 4—figure supplement 2. (A) EdU staining of blastocysts exposed to 5-aza-dC from the 8-cell to blastocyst stage. Right panel: the percentage of EdU-positive cells. (B) The total cell number (left panel) and the ratio of ICM/TE (right panel) of blastocysts treated with or without 5-aza-dC. (C) The total ATP production (left panel) and OXPHOS-dependent ATP production (right panel) of blastocysts treated with or without 5-aza-dC. All data are presented as the mean ± SD of at least three independent experiments. $^{*}P < 0.05$, $^{**}P < 0.01$. ns, not significant. Scale bars: 50 μm (A, B).

Supplemental Tables (separate files)

Supplemental Table S1. Primers sequences used in this study.

Figure 1

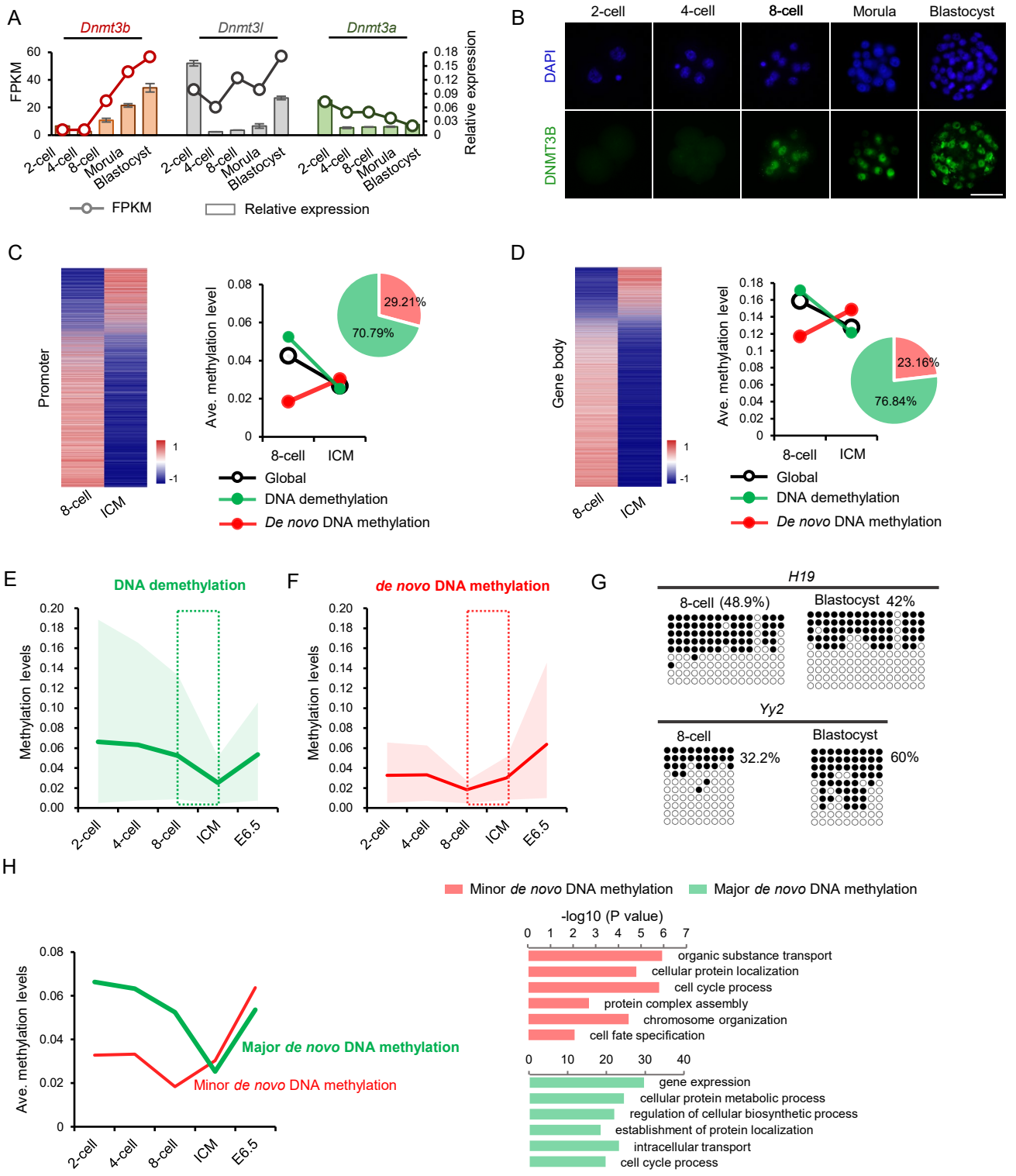
A
Dnmt3b
Dnmt3l
Dnmt3a
FPKM
Relative expression
2-cell
4-cell
8-cell
Morula
Blastocyst
FPKM
Relative expression
B
2-cell
4-cell
8-cell
Morula
Blastocyst
DAPI
DNMT3B
C
Promoter
8-cell
ICM
Ave. methylation level
29.21%
70.79%
Global
DNA demethylation
De novo DNA methylation
D
Gene body
Ave. methylation level
23.16%
76.84%
Global
DNA demethylation
De novo DNA methylation
E
DNA demethylation
Methylation levels
2-cell
4-cell
8-cell
ICM
E6.5
F
de novo DNA methylation
Methylation levels
G
H19
8-cell (48.9%)
Blastocyst 42%
Yy2
8-cell
32.2%
Blastocyst
60%
H
Ave. methylation levels
Major de novo DNA methylation
Minor de novo DNA methylation
Minor de novo DNA methylation
Major de novo DNA methylation
-log10 (P value)
organic substance transport
cellular protein localization
cell cycle process
protein complex assembly
chromosome organization
cell fate specification
gene expression
cellular protein metabolic process
regulation of cellular biosynthetic process
establishment of protein localization
intracellular transport
cell cycle process

Figure2

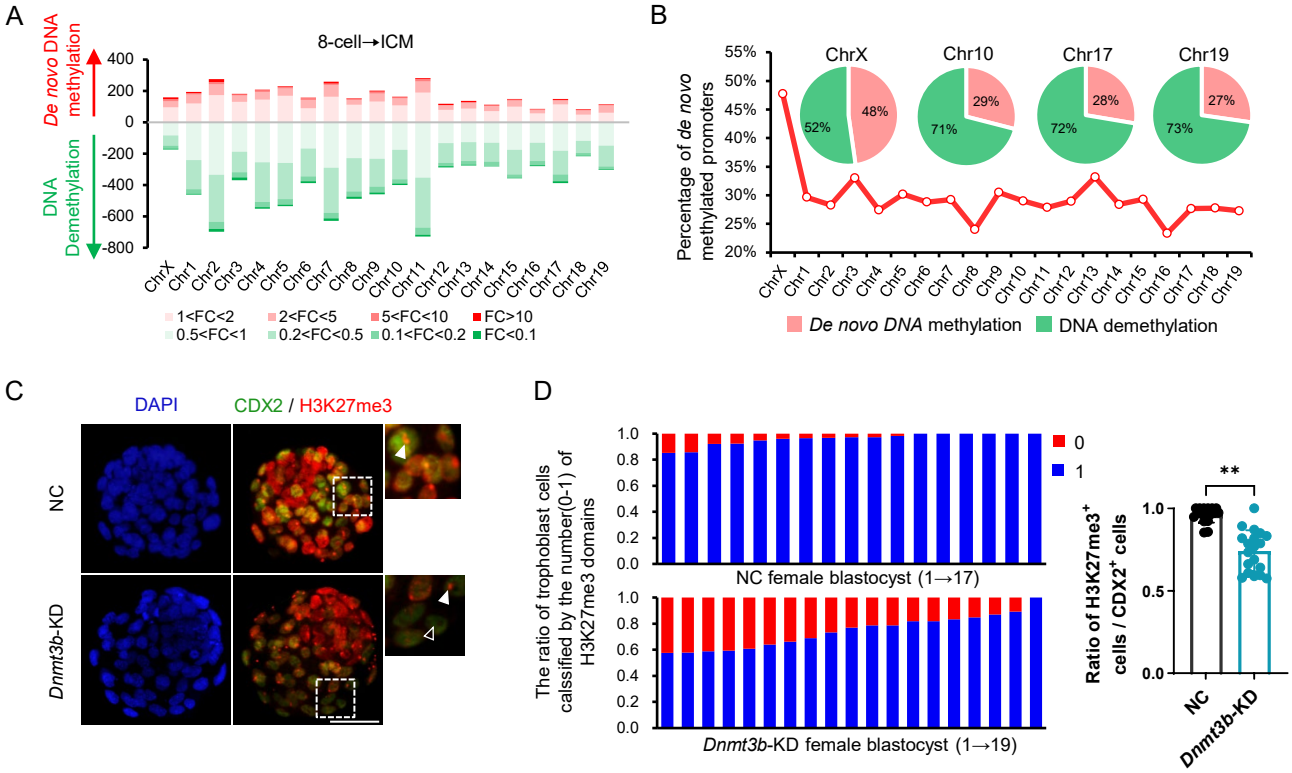
A
8-cell→ICM
De novo DNA methylation
DNA Demethylation
400
200
0
-200
-400
-600
-800
ChrX Chr1 Chr2 Chr3 Chr4 Chr5 Chr6 Chr7 Chr8 Chr9 Chr10 Chr11 Chr12 Chr13 Chr14 Chr15 Chr16 Chr17 Chr18 Chr19
1<FC<2
2<FC<5
5<FC<10
FC>10
0.5<FC<1
0.2<FC<0.5
0.1<FC<0.2
FC<0.1
B
Percentage of de novo methylated promoters
55%
50%
45%
40%
35%
30%
25%
20%
ChrX
Chr10
Chr17
Chr19
52%
48%
71%
29%
72%
28%
73%
27%
De novo DNA methylation
DNA demethylation
C
DAPI
CDX2 / H3K27me3
NC
Dnmt3b-KD
D
The ratio of trophoblast cells calssified by the number(0-1) of H3K27me3 domains
1.0
0.8
0.6
0.4
0.2
0.0
0
1
NC female blastocyst (1→17)
Dnmt3b-KD female blastocyst (1→19)
Ratio of H3K27me3+ cells / CDX2+ cells
**
NC
Dnmt3b-KD

Figure 3

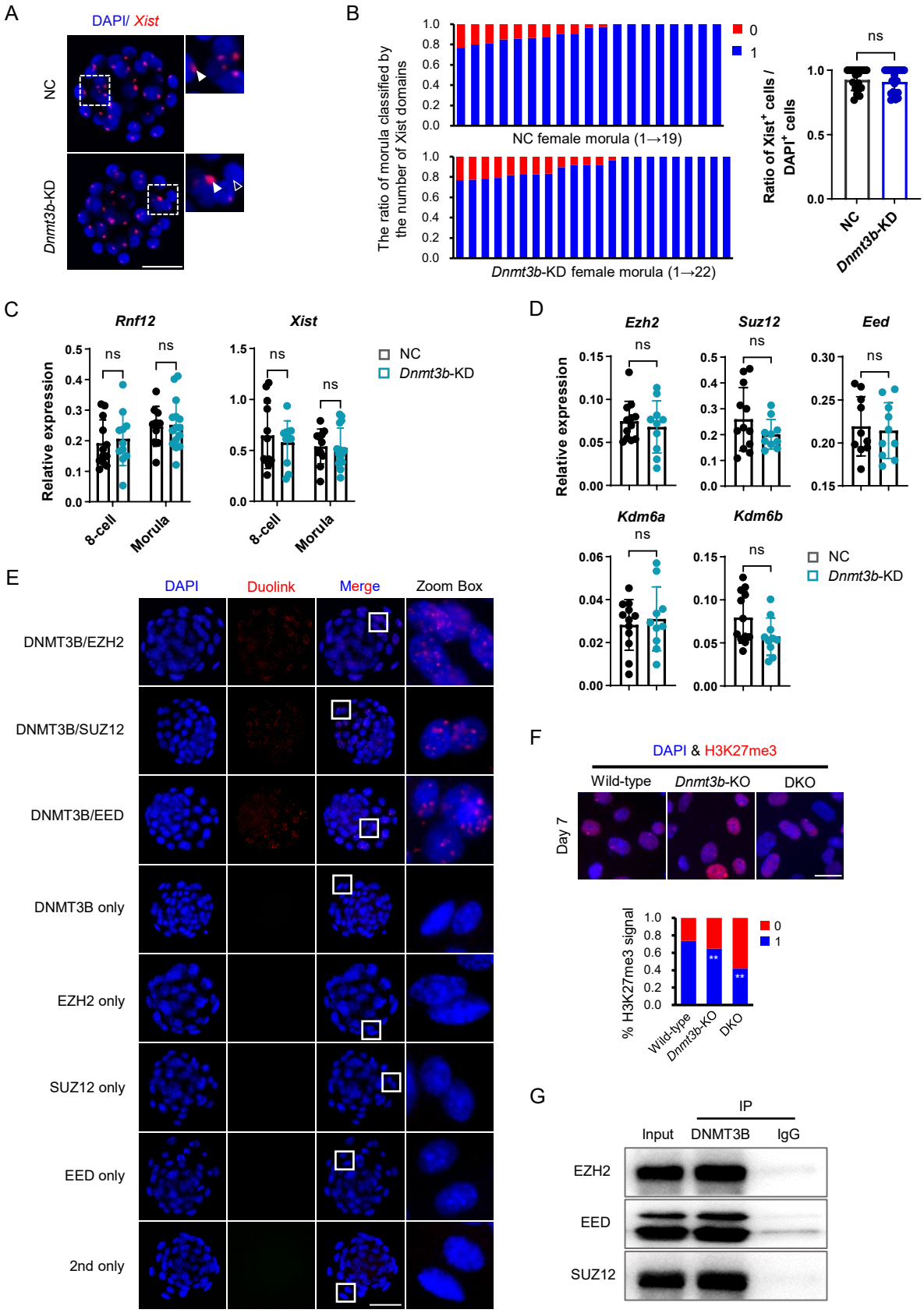
A
DAPI/ Xist
NC
Dnmt3b-KD
B
The ratio of morula classified by the number of Xist domains
NC female morula (1→19)
Dnmt3b-KD female morula (1→22)
0
1
ns
Ratio of Xist+ cells / DAPI+ cells
NC
Dnmt3b-KD
C
Rnf12
Xist
Relative expression
ns
8-cell
Morula
NC
Dnmt3b-KD
D
Ezh2
Suz12
Eed
Kdm6a
Kdm6b
Relative expression
ns
NC
Dnmt3b-KD
E
DAPI
Duolink
Merge
Zoom Box
DNMT3B/EZH2
DNMT3B/SUZ12
DNMT3B/EED
DNMT3B only
EZH2 only
SUZ12 only
EED only
2nd only
F
DAPI & H3K27me3
Wild-type
Dnmt3b-KO
DKO
Day 7
% H3K27me3 signal
0
1
**
G
IP
Input
DNMT3B
IgG
EZH2
EED
SUZ12

Figure 4

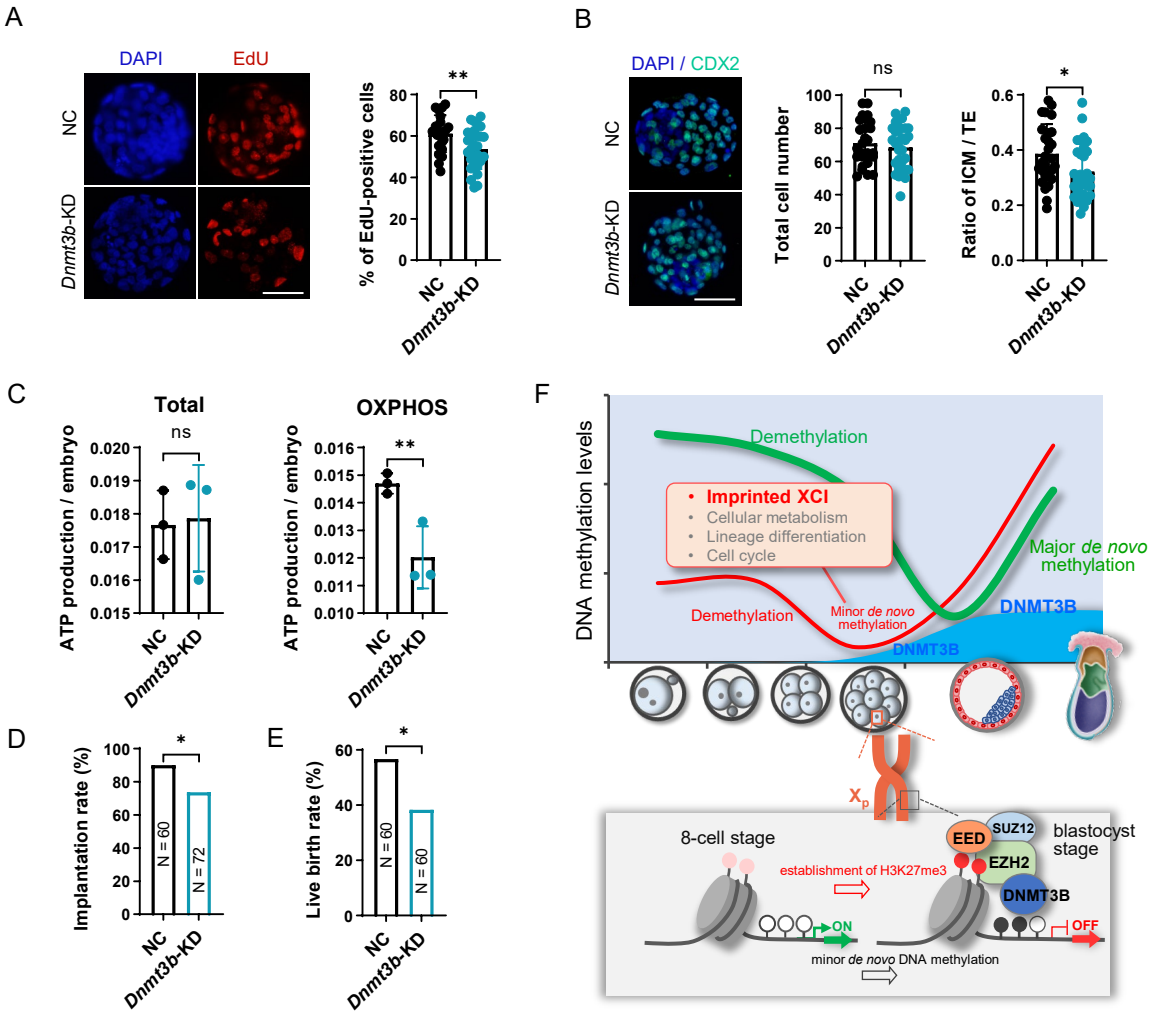
A
DAPI
EdU
NC
Dnmt3b-KD
% of EdU-positive cells
**
B
DAPI / CDX2
Total cell number
ns
Ratio of ICM / TE
*
C
Total
OXPHOS
ATP production / embryo
D
Implantation rate (%)
N = 60
N = 72
E
Live birth rate (%)
F
DNA methylation levels
Demethylation
Imprinted XCI
Cellular metabolism
Lineage differentiation
Cell cycle
Major de novo methylation
Minor de novo methylation
DNMT3B
Xp
8-cell stage
blastocyst stage
EED
SUZ12
EZH2
establishment of H3K27me3
ON
OFF
minor de novo DNA methylation

Figure 1—figure supplement 1

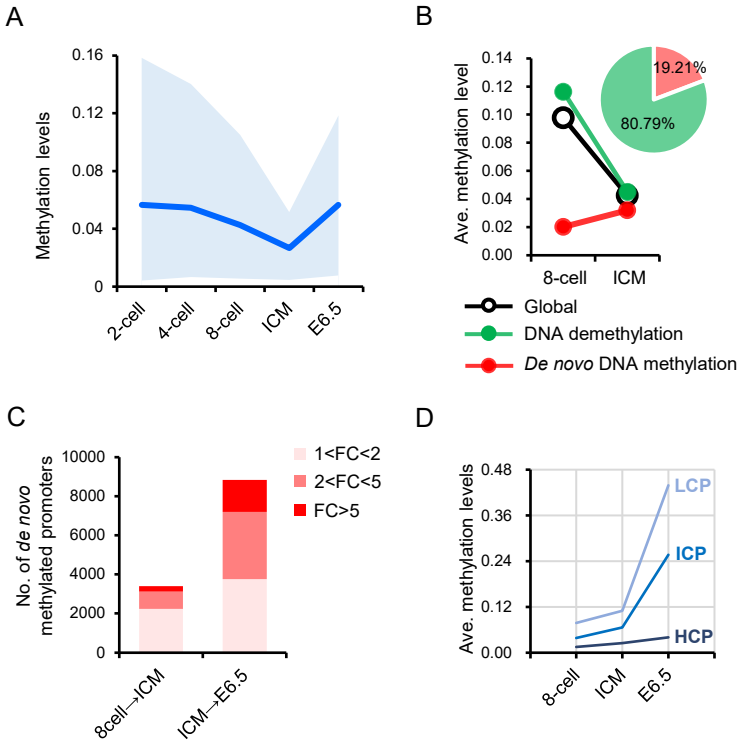

Figure 2—figure supplement 1

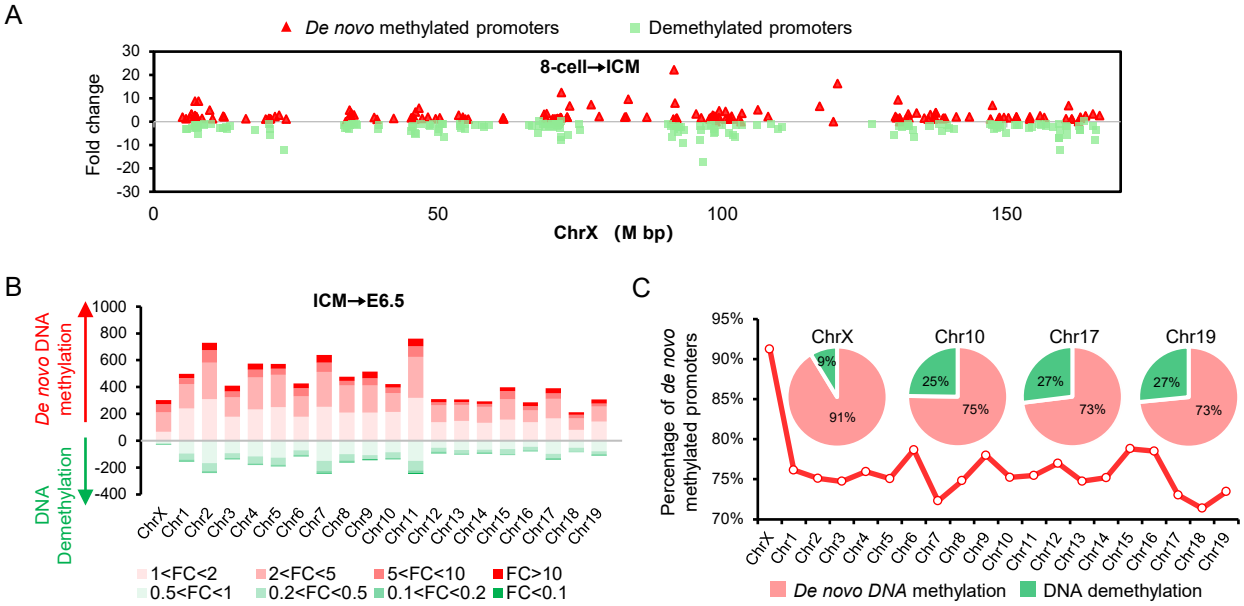

Figure 2—figure supplement 2

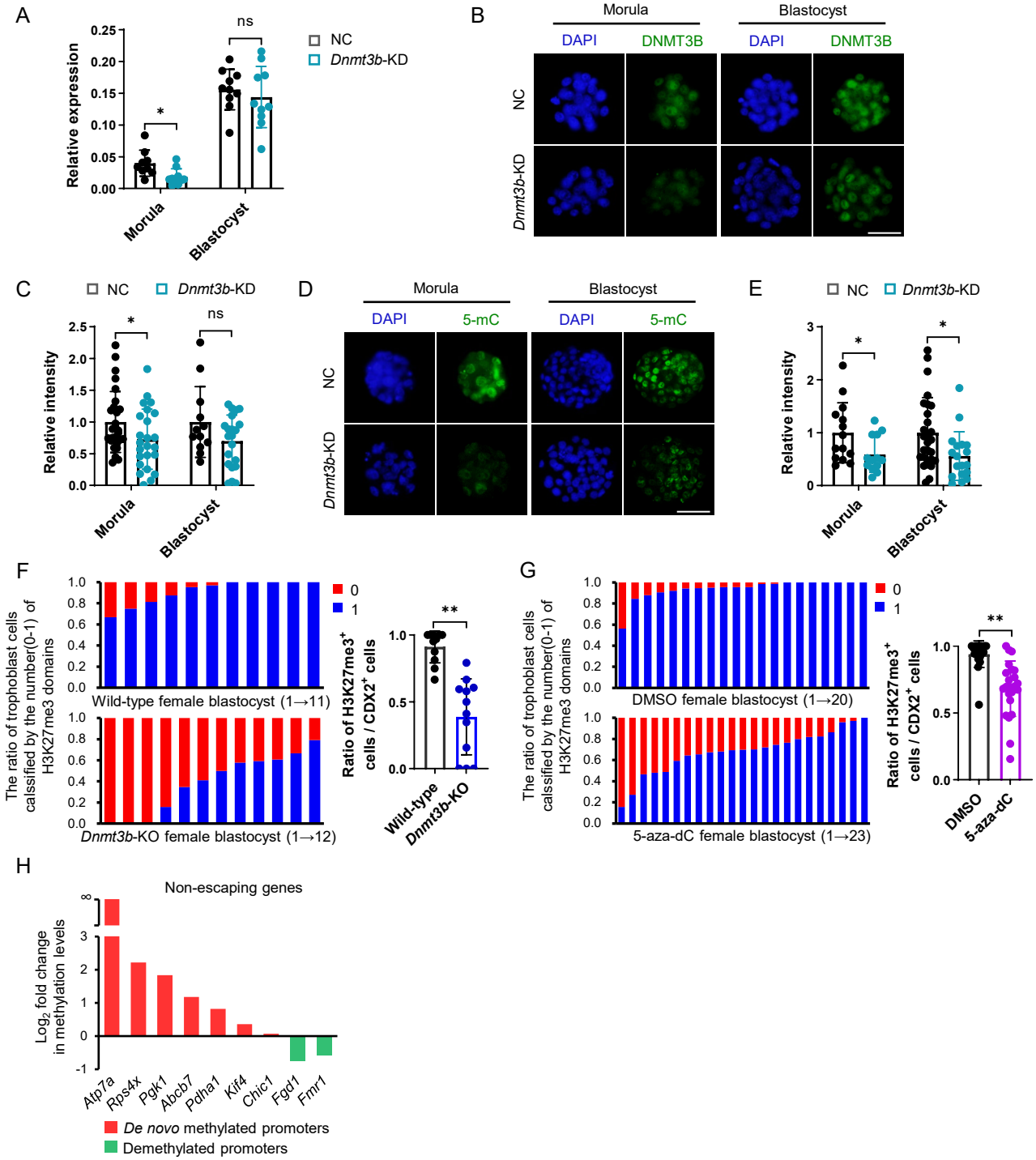

Figure 3—figure supplement 1

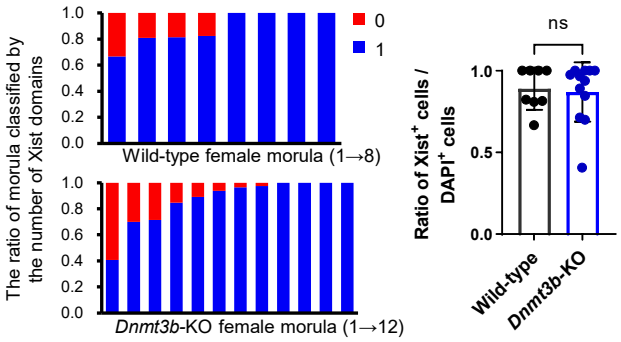

Figure 3—figure supplement 2

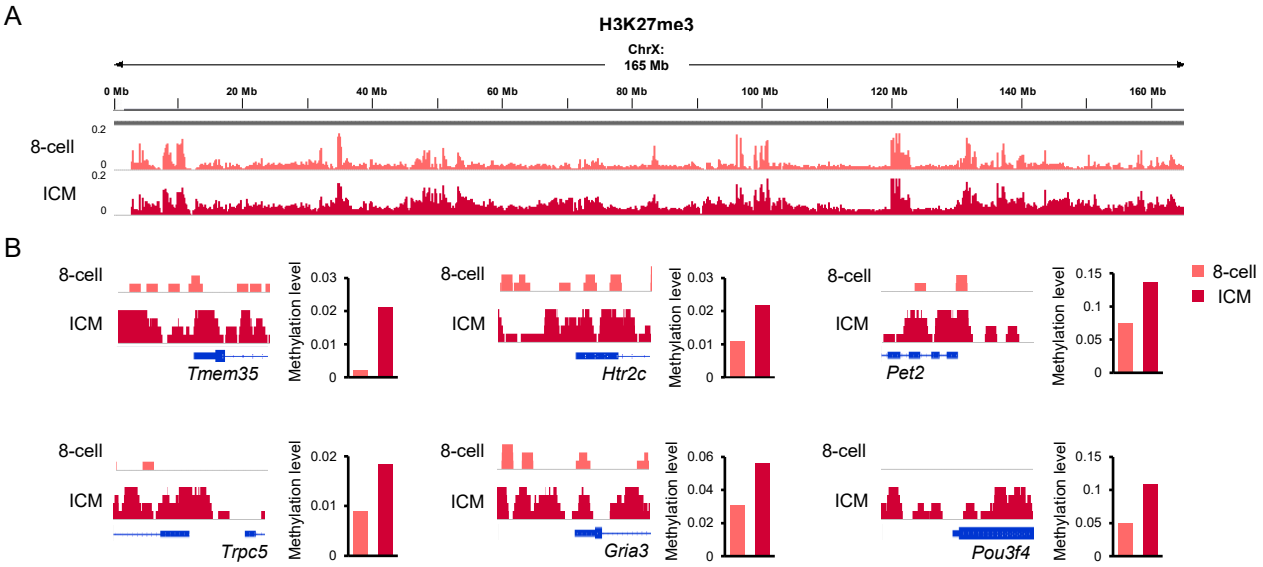

Figure 3—figure supplement 3

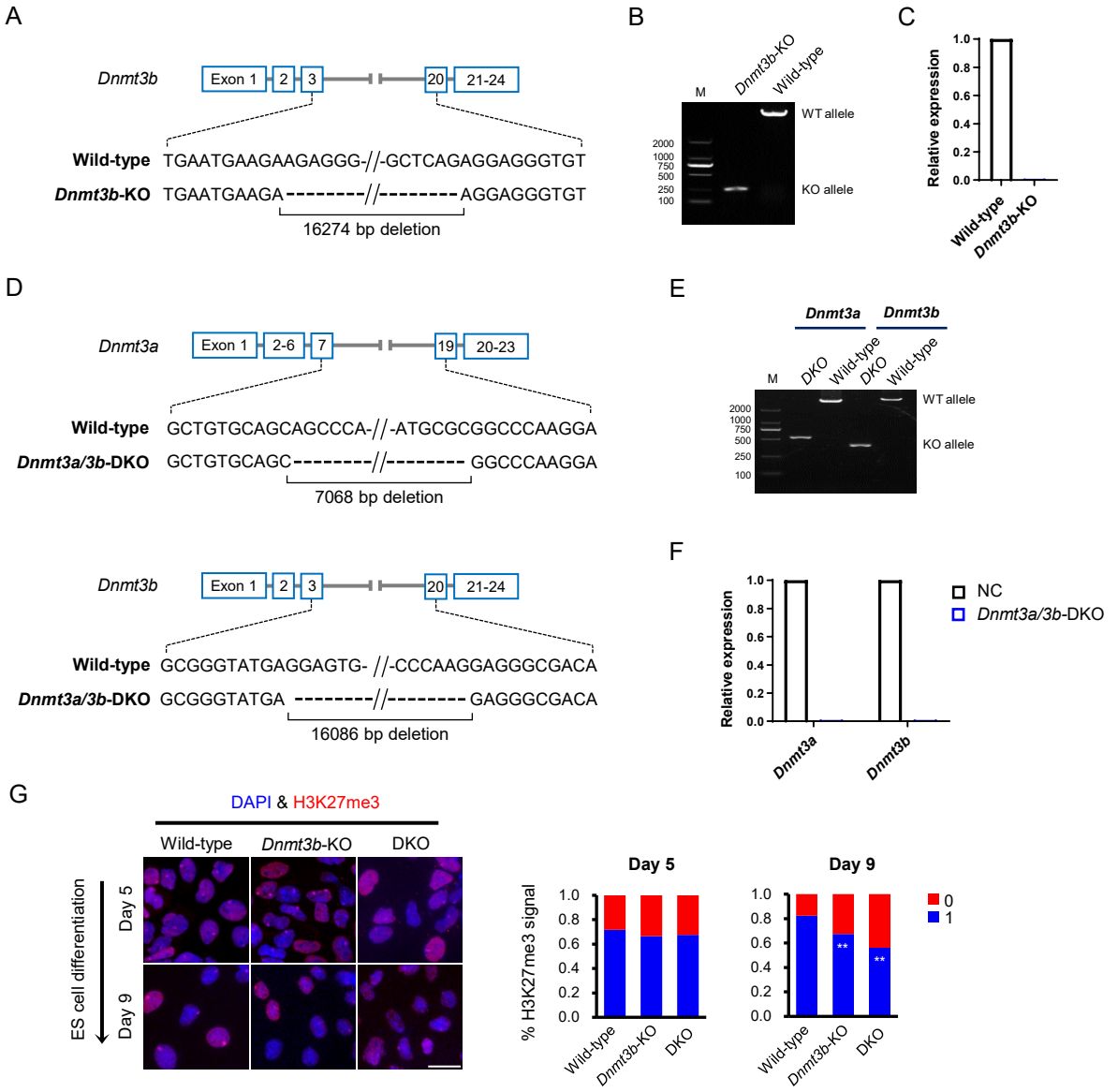

Figure 4—figure supplement 1

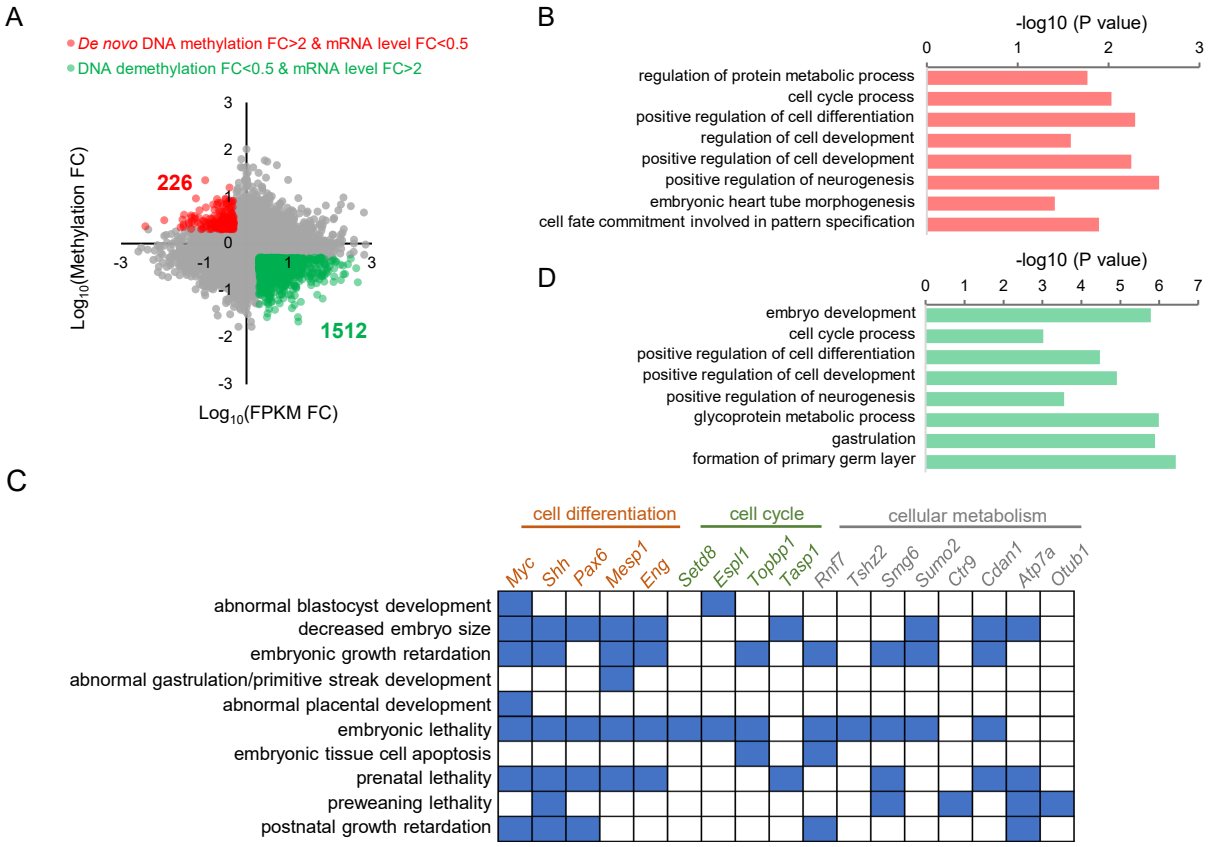
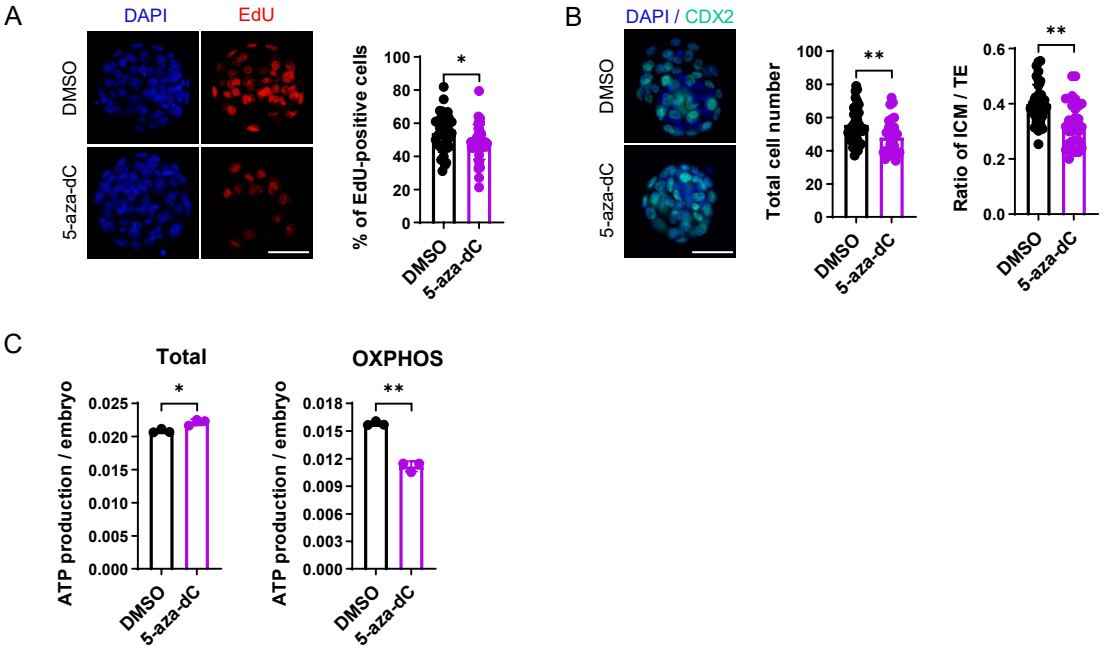
Figure 4—figure supplement 2